Ceramics international, 42(1B), pp1679-1687
DOI: 10.1016/j.ceramint.2015.09.122

Enhanced energy-storage performance and electrocaloric effect in compositionally graded $Pb_{(1-3x/2)}La_xZr_{0.85}Ti_{0.15}O_3$ antiferroelectric thick films

Ye Zhao[1], Xihong Hao[*,1], and Qi Zhang[2,3]

1-School of Materials and Metallurgy, Inner Mongolia University of Science and Technology, Baotou 014010, China

2-State Key Laboratory of Advanced Technology for Materials Synthesis and Processing, Wuhan University of Technology, Wuhan 430070, Hubei, China

3-Department of Manufacturing and Materials, Cranfield University, Cranfield, Bedfordshire, MK43 0AL, UK

Abstract: The compositionally graded multilayer $Pb_{(1-3x/2)}La_xZr_{0.85}Ti_{0.15}O_3$ (PLZT) antiferroelectric (AFE) thick films were deposited on $LaNiO_3$/Si (100) substrates by using a sol-gel method. The effect of gradient sequence on dielectric properties, energy-storage performance, and electrocaloric effect (ECE) were investigated in detail. It is found that the compositionally graded films exhibited the significant enhancement in dielectric properties, energy-storage performance and ECE, which was, in contrast to the single-composition PLZT film, contributed by the strain and the gradient of polarization near the interfaces between the adjacent layers. Therecoverable energy-storage density of 44 J/cm^3 and efficiency of 71% were obtained in the up-graded PLZT AFE thick film at 1950 kV/cm. A giant reversible adiabatic temperature change of ΔT = 28 ^{o}C at room temperature at 900 kV/cm were also achieved in the up-graded film. Moreover, all the thick films displayed a small leakage current density below 10^{-6} A/cm^2 at room temperature. Thus, the compositionally graded PLZT AFE thick films with a large recoverable energy-storage density and a giant ECE are potential candidate for the applications in high energy-storage density capacitors and cooling devices.

Keywords: Compositionally gradient; PLZT thick films; Energy-storage performance; ECE

*Corresponding author: xhhao@imust.cn; Tel: +86-472-5951572; Fax: +86-472-5951571

1 Introduction

Dipoles in the antiferroelectrics (AFEs) are alternatively aligned in the opposite directions and thus no net spontaneous polarization exists. In a AFE, a ferroelectric state could be induced under an electric field. However, the induced FE phase is not stable, and could return to AFE state under the change of electric field, temperature or stress. This phase switching process is accompanied by double hysteresis loops of polarization vs electric field, considerable pyroelectric coefficient, large strain, high energy-storage density, and large electrocaloric effect (ECE) [1-2]. Hence, AFEs could become the most promising candidates in high-strain transducers, high energy-storage capacitors and cooling devices [3-6]. Recently, AFEs with high energy-storage density and large ECE have received intensive studies due to both fundamental scientific interest and practical devices [1,7].

However, currently the energy-storage behaviors and ECE of lead-based AFEs in bulk ceramics and thin films (< 1 μm) have received increasing attention. The energy-storage performance and ECE of bulk ceramics both are very small because bulk ceramics cannot withstand a high operating voltage. For example, the maximum energy-storage density and ECE obtained in the AFE bulk ceramics are only 2.75 J/cm^3 and 2.5 K, respectively [8,9]. In addition, the bulk ceramics are usually not compatible with the semiconductor integrated circuit technology, which also make them unsuitable in practical applications. Although thin films possess higher breakdown electric field and are easily integrated with semiconductor technology, their overall stored energy and heat-sinking capacity are small due to their mass limitations. For instance, a large energy-storage density and ECE of 61 J/cm^3 and 11.4 K were reported in $Pb_{0.96}La_{0.04}Zr_{0.98}Ti_{0.02}O_3$ and $PbZrO_3$ thin films [1,10]. Therefore, thick films (1-10 μm) might provide a possible solution of high breakdown filed and large

overall volume by overcoming the shortcomings of both bulk ceramics and thin films and meet the requirements of applications in high energy-storage capacitors and cooling devices. An energy-storage density of as high as 56 J/cm^3 in 3.3 μm thick PLZT AFE films was reported by Hao *et.al.* [11]. Moreover, an ECE of ΔT = 3.8 ^{o}C and an electrocaloric coefficient$\Delta T/\Delta E$ of 0.048 at 32 ^{o}C were also received during AFE-FE transition in 1.0-μm-thick PLZST AFE films [12].

Although a few works on the energy-storage performance and ECE of AFE films have been carried out, these studies are mainly focused on chemical composition selection and breakdown-field improvement. In fact, the compositionally graded structure is useful for improving the many properties of AFEs in terms of dielectric properties, saturation polarization and pyroelectric coefficient. It was reported that the dielectric constant and polarization of $Ba_{0.80}Sr_{0.20}Ti_{1-x}Zr_xO_3$ compositionally graded films were larger than those of the single-layer film and increased with the increase of the gradient of compositions. The improved electrical properties in compositionally graded films are believed to be caused by the strain and the gradient of polarization near the interfaces between the adjacent layers [13-16]. However, the compositionally graded AFEs for the energy-storage performance and ECE were rarely investigated systematically, especially compositionally graded AFE thick films.

Thus, in this work, 1.0-μm compositionally graded multilayer $Pb_{1-3x/2}La_xZr_{0.85}Ti_{0.15}O_3$ AFE thick films were fabricated via a sol-gel method, and their energy-storage performance and ECE were investigated. The aim of this work is to obtain a large energy-storage density and ECE by the proper control of the grading sequence.

2 Experimental procedures

The $Pb_{1-3x/2}La_xZr_{0.85}Ti_{0.15}O_3$ (PLZT 100/85/15, x = 0.08, 0.11, and 0.14) precursor solutions

were synthesized using lead acetate trihydrate, lanthanum acetate, titanium isopropoxide and zirconium isopropoxide as the starting raw materials. Glacial acetic and deionized water were used as solvents. Lactic acid functioned as catalyzer and chelation agent was added into the solution in the ratio of one mole of lactic acid to one mole of lead. In order to improve the mechanical properties of the gel film, ethylene glycol was also added into the solution in the ratio of one mole of ethylene glycol to one mole of lead. The concentration of the precursor solution was 0.5 M with a 20 mol% of excess Pb in order to compemsate the lead loss during annealing and to prevent the formation of pyrochlore phase in the film. The conductive $LaNiO_3$ (LNO) films with a thickness of about 400 nm were chosen as bottom electrodes, which were prepared on Si (100) substrates by the chemical solution deposition route and as described in Ref. 17. The obtained LNO films showed a (100) growth orientation.

After aged for 24 h, PLZT AFE films were deposited on LNO/Si (100) substrates through a multiple-step spin-coating technique. Each layer was spin coated at 3000 rpm for 40 s. In order to reduce the formation of cracks, every wet film was first dried at 350 ^{o}C for 10 min and subsequently pyrolyzed at 600 ^{o}C for 10 min. The spin-coating and heat-treatment were repeated several times to obtain the desired thickness. A capping layer of 0.4 M PbO precursor solution which was prepared from lead acetate trihydrate, was added before the films went through a final anneal at 700 ^{o}C for 30 min to form the perovskite phase. This capping layer served the purpose of preventing excessive lead loss, thereby ensuring the formation of a single perovskite phase of the films. The final thickness of the three kinds of films was about 1.0 μm, determined from the SEM cross-sectional images. For convenience, the films with La content varying from 8 mol% at the substrate interface to 14 mol% at the top surface were named “up-graded (UG)” films, whereas films with opposite gradient were

called “down-graded (DG)” films. For comparison, the film with single composition (SC) of PLZT 11/85/15 was also prepared. The layer thickness of each composition was equal. The schematic diagrams of the SC, UG, and DG PLZT films are given in Fig. 1.

The crystallinity and the microstructure of the thick films were analyzed by X-ray diffraction (XRD Bruker D8 Advanced Diffractometer, German) and field-emission scanning electron microscopy (FE-SEM ZEISS Supra 55, German), respectively. For the measurements of electrical properties, gold pads of 0.20 mm in diameter were coated on the surface as top electrodes by using a dc sputtering method. The frequency and temperature-dependent dielectric properties of the thick films were measured by using a computer-controlled Agilent E4980A LCR analyzer. The polarization-electric field hysteresis loops (*P*-*E*) and the leakage current characteristic of the thick films were measured by a Radiant Technology Ferroelectric tester with high-voltage power supply (Trek Inc., Media, NY).

3 Results and discussion

Fig. 2 presents the XRD patterns of the UG, DG, and SC PLZT AFE thick films grown on LNO/Si (100) substrates. From the XRD patterns, it is found that all the AFE thick films display a unique perovskite structure without any other phases, and pseudocubic (100), (110), and (111) are detected. Clearly, the phase structure of the AFE thick films is not affected by the composition gradient sequence of the PLZT AFE thick films. The grain size of 51.4, 65.4, and 58.2 nm are calculated using the Software JADE for the UG, DG and SC AFE thick films, respectively. Moreover, all the thick films grown on (100)-preferred LNO bottom electrodes also showed (100)-preferred orientation, which was ascribed to the same grown orientation and small mismatch between the AFE films and LNO bottom electrodes [18].

The FE-SEM images of surface and cross-sectional morphologies of the UG, DG, and SC PLZT AFE thick films are given in the Fig. 3(a-f). As can be seen in these figures, all the microstructures of the thick films are dense and compact, which was ascribed to the two-step heat-treatment during the thick films preparation. The cross-sectional morphologies of these thick films present a column-like structure, indicating that the nucleation and growth of the crystals may initiate from the bottom electrodes [19]. The films share the same thickness of 1.0 μm.

Frequency-dependent dielectric constant and dielectric loss for these AFE thick films measured at room temperature and over 1-1000 kHz are plotted in Fig. 4. It can be seen that with the increase of frequency, a gradual degradation of dielectric constants is observed for all the films, which was induced by the different response times for the various dipoles [20]. It is found that the dielectric constant of thick films is strongly dependent on their grading sequence. The UG film possesses the highest dielectric constant, followed by the DG and then the SC thick films. For example, it is clear that the values of dielectric constant at 100 kHz are 865, 701, and 587 for the UG, DG, and SC PLZT AFE thick films, respectively. The same results were also reported in the $Pb(Zr_xTi_{1-x})O_3$ compositionally graded films, which were related to the strain and the gradient of polarization near the interfaces between the adjacent layers [21]. However, the dielectric loss of these thick films is slightly affected by their composition gradient sequence, and all the thick films share the similar values below 0.04 at 100 kHz. In the measurement range, the dielectric loss increase with the increase of frequency, which were attributed to the polarization relaxation.

Fig. 5 shows the electric field-dependent dielectric constant (ε_r-E) of the UG, DG and SC PLZT AFE thick films, which were measured at 100 kHz at room temperature. The dc field is stepped at a time lag of 0.5 s according to the following measurement mode: zero to E_{max}, E_{max} to - E_{max}, and -

E_{max} to zero. Clearly, both ε_r-E curves illustrate a double butterfly behavior, corresponding to the phase transition between AFE to FE as the function of dc electric field. The dielectric constant sharply increases at the AFE-FE transition and then drops when the curve saturated. From peaks of the ε_r-E curves, the magnitude of phase switching field could be determined. The forward switching field for the AFE-FE transition (E_F) and the reverse switching field for FE-AFE transition (E_{AF}) are observed at 160, 175, 155 kV/cm and 110, 135, 120 kV/cm in the UG, DG and SC PLZT AFE thick films, respectively. The various AFE-FE phase transitions of the thick films probably contribute to the difference in the substrate constraint and the gradient of polarization caused by the composition and the gradient sequence [22].

Fig. 6 illustrates the temperature-dependent dielectric constant of these samples measured at 100 kHz with a heating rate of 3 ^{o}C/min. It is clearly seen that the dielectric constant increased gradually to maximum value at the phase transition temperature (T_m), and then decreased smoothly. The broad nature of the plots indicates a diffused phase transition from AFE to paraelectric (PE) phase. T_m of SC PLZT AFE thick films is about 120 ^{o}C, while T_m of the UG and DG thick films was 136 ^{o}C and 118 ^{o}C, respectively. For the compositionally graded thick films, the shift of T_m is believed to be attributed to the presence of the misfit strain among the interfaces of layers. Because the ionic radii of Pb^{2+} (0.149 nm) is larger than that of La^{3+} (0.136 nm), the lattice constant of PLZT AFE thick film decreases with the increase ratio of La. The lattice constant of $Pb_{0.88}La_{0.08}Zr_{0.85}Ti_{0.15}O_3$ is greater than that of $Pb_{0.79}La_{0.14}Zr_{0.85}Ti_{0.15}O_3$, which makes the UG PLZT AFE thick film suffers from a tensile misfit strain. Conversely, the DG thick film suffers from a compressive misfit strain. In general, if there is a tensile strain along the in-plane direction inside the film, T_m is likely to shift towards to the high temperature direction, whereas the compressive strain

results in the opposite effect [18,23].

Fig. 7 shows the room temperature polarization-electric field hysteresis loops of the UG, DG and SC PLZT AFE thick films, which were measured at 1 kHz and at 900 kV/cm. It can be seen that these thick films show a typical AFE behavior with double *P-E* loop and double butterfly character of dielectric constant (Fig. 5). Apparently, the maximum polarization (P_{max}) of the thick films is strongly dependent on their grading sequence, while the remnant polarization (P_r) is only slightly affected. Under the measurement condition, the values of P_{max} are 73 μC/cm^2, 63μC/cm^2, and 54 μC/cm^2 for the UG, DG, and SC PLZT AFE thick films, respectively. The UG film possesses the largest polarization, and SC film has the smallest value, which coincides with their dielectric properties due to the strain and the gradient of polarization. The larger P_{max} would lead to higher recyclable energy-storage density and larger ECE could possibly be obtained in these films.

Fig. 8(a) presents the recyclable energy-storage density and energy-storage efficiency of these samples as a function of the operating electric fields, which were measured from 200 kV/cm to their maximum electric field at 1 kHz and at room temperature. Generally, the recoverable energy-storage density *W* could be estimated from the *P-E* loops, which is calculated with the equation as below:

$$W = \int_{P_r}^{P_{\max}} EdP \,, \tag{1}$$

where *E* is the applied electric field, *P* the polarization, P_r remanent polarization and P_{max} the maximum polarization. According to equation (1), materials with smaller P_r, larger P_{max} and higher breakdown strength are more suitable for energy storage. In all cases, the recoverable energy-storage density increase with the increase of the electric field, and the higher energy-storage density can be obtained under the higher breakdown electric field. As desired, the energy-storage density is dramatically different for these samples. Clearly, it can be seen that the UG thick film displays the largest *W* values, and the SC thick film has the lowest values over the measurement range. For

example, the W values at their corresponding maximum electric field are 44, 30, and 22 J/cm^3 for the UG, DG and SC PLZT AFE thick films, respectively. The improved recoverable energy-storage properties of compositionally graded thick films attribute to the high P_{max} and good endurance of electric field. For the application of dielectric capacitors in practice, a higher energy-storage efficiency η is also always desired. The energy-storage efficiency η is calculated as the following formula:

$$\eta = \frac{W}{W + W_{loss}}, \tag{2}$$

where W_{loss} is the energy loss density, calculated by the numerical integration of closed area of the hysteresis loops. Obviously, different from the W values, the η values of thick films are less affected by their grading sequence. The η values are similar for these thick films and are slightly declined as the increase of the measured electric field. For example, the η value of UG thick film is changed from 86% to 71% as the electric field increases from 200 to 1950 kV/cm. The temperature-dependent stability of the energy-storage performance is also a very important parameter for the capacitor application. To investigate the temperature-dependent stability of the capacitors, the energy-storage density and the energy-storage efficiency measured at 1 kHz in the temperature ranging from 20 to 150 ^{o}C are presented in Fig. 8(b). In order to avoid electric breakdown at higher temperature, the measurements of *P-E* loops for all the samples were carried out at a lower electric field of E = 900 kV/cm. Evidently, all the curves are only slightly varied in the measurement range. For example, the W value for the UG thick film are varied from 19.2 J/cm^3 to 17.9 J/cm^3, and the corresponding η value are varied from 75% to 77%, indicating good temperature stability of the energy-storage performance.

ECE is a temperature change (ΔT) in a polarizable dielectric material by virtue of the change in entropy (ΔS) upon the application of or removal of an electric field under adiabatic conditions. The reversible adiabatic in ΔT and ΔS for a material of density (ρ) with heat capacity (C) are expressed by

[24]:

$$\Delta T = -\frac{1}{C\rho}\int_{E_1}^{E_2} T\left(\frac{\partial P}{\partial T}\right)_E dE\,, \tag{3}$$

$$\Delta S = -\frac{1}{\rho}\int_{E_1}^{E_2}\left(\frac{\partial P}{\partial T}\right)_E \mathrm{d}E\,, \tag{4}$$

assuming the Maxwell relation $\left(\frac{\partial P}{\partial T}\right)_E = \left(\frac{\partial S}{\partial E}\right)_T$, where T is operating temperature, P is maximum polarization at applied electric field E, and E_1 and E_2 are the initial and final applied electric field, respectively. Fig. 9(a) shows the adiabatic temperature change ΔT of the UG, DG and SC PLZT AFE thick films under ΔE = 900 kV/cm. Evidently, compared with the SC thick film, the compositionally graded thick films have larger ΔT at room temperature. The specific heat capacity C = 330 $J \cdot K^{-1} \cdot kg^{-1}$ and the theoretical density ρ = 7.9 $g \cdot cm^{-3}$ are selected for the films, which was reported in previous work [25,26]. Here E_1 = 0 and $E_2 = E$; thus ΔE is equal to E. As shown in the figure 9(a), the UG, DG and SC films show the same changing tendency in the operating temperature-dependent ΔT curves. Under the measurement condition, ΔT of the UG, DG and SC PLZT AFE thick films are 28, 20, and 7 ^{o}C at room temperature, respectively, which is induced by the phase transition of FE-AFE. With the operating temperature increasing, the ΔT firstly decreases, indicating a reduction of entropy change between AFE and FE phase transition. With the further increase of temperature, a peak of ΔT = 8, 11, and 7 ^{o}C is detected at 185, 156, and 142 ^{o}C at E = 900 kV/cm, which is believed to be caused by the AFE-PE phase transition. The temperature corresponding to the peak of ΔT is slightly below its T_c, which is consistent with that previously reported by Tatsuzaki, because the spontaneous value of P greatly changes with temperature below T_c [48]. In fact, ECE can occur both above and below T_c, but the microscopic models of ECEs are not well established [14]. It is reported that the maximum ΔT under saturation can be estimated from the dielectric data, such as the saturation polarization P_s, effective Curie constant Θ, the number of possible polar states φ and the specific heat C of the material. Based on thermodynamic and statistical mechanics analyses, Pirc *et. al.* derived

the following expression for the upper bound on the value of ΔT in the saturation limit:[27]

$$\Delta T_{sat} = \frac{T \ln \varphi}{3\varepsilon_0 \Theta C} P_s^2 \quad (5).$$

Evidently, the materials, which possess a large P_s, high φ, small Θ, and small C would have giant ECE. The values of P_s, φ, Θ, C, and T for the UG, DG and SC PLZT AFE thick films are list in the Table 1. These films share the same values of both φ and C. Therefore, P_s^2/Θ is critical factor of ECE in the films at the room temperature. Due to the largest the value of P_s^2/Θ, an enhanced ECE is obtained in the UG films. With the increase of the measurement temperature, another peak value ΔT =10, 18, and 11^{o}C of the UG, DG, and SC thick films are observed at 115, 111, and 113 ^{o}C, respectively. The peaks of ΔT of all the thick films are corresponding to the changing tendency of their T_m and lower than their T_m. Moreover, it could be found from these figures that all the curves display diffused character, indicating that giant ECE of these films are obtained in a wide operating temperature range. Fig. 9(b) gives the corresponding adiabatic ΔS of the UG, DG, and SC PLZT AFE thick film under different electric field. Obviously, the maximum values of ΔS are 31, 23, and 8 $J \cdot K^{-1} \cdot kg^{-1}$ of the UG, DG, and SC PLZT AFE thick films at room temperature at 900 kV/cm, respectively. The adiabatic ΔS is also an important parameter of ECE based cooling devices in practical applications.

Fig. 10(a) illustrates the coefficient of performance (*COP*) of thick films at 900 kV/cm. *COP* allows evaluation of cooling cycle performance and assessment of its efficiency, where *COP* is defined as the relationship between the isothermal heat *Q* and *W*, expressed as [28]:

$$COP = \frac{|Q|}{|W|} = \frac{|\Delta S \times T|}{|W|} \quad (6).$$

Based on above formulas, the calculated *COP* values of the UG, DG, and SC PLZT AFE thick films are 3.8, 3.1, and 1.2 at room temperature and at 900 kV/cm. The maximum *COP* is found to be 3.8 of the UG thick film, which is larger than that (*COP* = 3.0) obtained in $PbZr_{0.95}Ti_{0.05}O_3$ film [25]. To

measure quantitatively how effective an applied electric field ΔE in generating ECE in the thick films, the ratio of $\Delta T/\Delta E$ has been introduced in earlier studies, as shown in the Fig. 10(b) [29]. In this work, this parameter is referred to as the electrocaloric coefficient. Clearly, the change of $\Delta T_{max}/\Delta E_{max}$ is in agreement with ΔT and *COP* of the thick film, as a temperature function. The value of $\Delta T_{max}/\Delta E_{max}$ for the UG, DG, and SC PLZT AFE thick films are 0.031, 0.023, and 0.008 K·cm/kV, respectively. The maximum $\Delta T_{max}/\Delta E_{max}$ of the UG film is 0.031 K·cm/kV at room temperature and at 900 kV/cm, which is higher than that ($\Delta T_{max}/\Delta E_{max}$ = 0.025 K·cm/kV) in $Pb_{0.88}La_{0.08}Zr_{0.85}Ti_{0.15}O_3$ thick film [26].

The Fig. 11(a) shows the current-time characteristics for dielectric relaxation current of these samples measured at room temperature and 400 kV/cm. The leakage current density shows strong initial time-dependence because of the dielectric polarization relaxation, which obeys the Curie-von Schweidler law as follows [30]:

$$J = J_s + J_0 \times t^{-n} \tag{7}$$

where J_s is the steady-state current density, J_0 is a fitting constant, t is the relaxation time in second, and n is the slope of the log-log plot. The possible mechanisms are associated with the Curie-von Schweidler law: space charge trapping, relaxation time distribution and electrical charge hopping [31]. It could be found that the leakage current density is affected by the compositional gradient sequence. The smaller leakage current is consistent with our previous reports on the lead-based AFE films [26]. By fitting the data into Eq. 7, the thick films grading sequence dependences of steady-state leakage current density were obtained and shown in the inset of Fig. 11(a), which are 3.22×10^{-7}, 7.59×10^{-7}, and 1.40×10^{-6} A/cm^2 for the UG, DG, and SC thick films, respectively. The smaller leakage currents yield negligible Joule heating (~ 10^{-5} K) and do not affect *P-E* results because currents of hundreds of μA are required to switch the measured polarizations at 1 kHz. Fig. 11(b) presents the current density-time characteristics of the thick films with x = 0.14 measured at

the temperature range of 25-200 ^{o}C and at 400 kV/cm. Clearly, the leakage current density of the sample increases with increasing temperature. The data were fit into the Arrhenius equation [32]:

$$J_s = C\exp\left(-\frac{E_a}{kT}\right) \quad (8)$$

where C is a constant, E_a is the activation energy, k is the Boltzmann constant, as shown in the inset of Fig. 11(b). The result yielded activation energy of ~0.45 eV, which is close to the reported results in PLZT films [32]. It is believed that the activation energy is within the range 0.32~0.49, the conduction performance of the thick films is attributed to the first-ionization of oxygen vacancies [33]. This result indicated that the films possess a good dielectric property even at higher temperature, which is favor to their application in high-power energy storage applications and high performance and practical ECE cooling devices.

4.1 Conclusions

In summary, compositionally graded PLZT AFE thick films with (100)-preferred orientation were prepared by using a sol-gel method. The dielectric properties, energy-storage performance and ECE of these thick films were strongly dependent on the gradient sequence of the composition. Compared with the SC thick film, the compositionally graded thick films possessed higher dielectric constant and larger saturation polarization. Hence, improved energy-storage performance and ECE were realized in the compositionally graded thick films. The maximum energy-storage density of 44 J/cm^3 and ECE of 28 ^{o}C were obtained in the UG PLZT AFE thick film. Meanwhile, all the thick films exhibited good energy-storage stability in the temperature range of 20 ^{o}C to 150 ^{o}C. Overall, the compositionally graded PLZT AFE thick films presented a large energy-storage density and a giant ECE, which is promising in designing energy-storage capacitors and cooling devices.

Acknowledgements

The authors would like to acknowledge the financial support the Program for New Century

Excellent Talents in University (2012), the National Natural Science Foundation of China under grant No. 51462027, the Ministry of Sciences and Technology of China through 973-project under grant No.2014CB660811, and the Innovation Program of Inner Monglia University of Science and Technology No. 2014QNGG01.

Reference

[1] Z.Q. Hu, B.H. Ma, R.E. Koritala, U. Balachandran, Temperature-dependent energy storage properties of antiferroelectric $Pb_{0.96}La_{0.04}Zr_{0.98}Ti_{0.02}O_3$ thin films, Appl. Phys. Lett. **104 (**2014) 263902.

[2] X.H. Hao, J.W. Zhai, L.B. Kong, Z.K. Xu, A comprehensive review on the progress of lead zirconate-based antiferroelectric materials, prog. Mater. Sci. **63 (**2014) 1-57.

[3] C.D. Campbell, J.D.V. Wyk, R. Chen, Experimental and theoretical characterization of an antiferroelectric ceramic capacitor for power electronics, IEEE Trans. Compon. Packag. Technol. **25** (2002) 211-216.

[4] M.S. Mirshekarloo, K. Yao, T. Sritharan, Large strain and high energy storage density in orthorhombic perovskite $(Pb_{0.97}La_{0.02})(Zr_{1-x-y}Sn_xTi_y)O_3$ antiferroelectric thin films, Appl. Phys. Lett. **97 (**2010) 142902.

[5] Z.K. Xu, W.H. Chan, Preparation and electrical properties of highly (111) oriented antiferroelectric PLZST films by radio frequency magnetron sputtering, Acta Materialia **55 (**2007) 3923-3928.

[6] M. Valant, Electrocaloric materials for future solid-state refrigeration technologies, Prog. Mater. Sci. **57** (2012) 980-1009.

[7] I. Burk, D.M. Smyth, Energy storage in ceramic dielectrics, J. Mater. Sci. **7** (1972) 339-343.

[8] L. Zhang, S. Jiang, Y. Zeng, M. Fu, K. Han, Q. Li, Q. Wang, G. Zhang, Y doping and grain size co-effects on the electrical energy storage performance of $(Pb_{0.87}Ba_{0.1}La_{0.02})$ $(Zr_{0.65}Sn_{0.3}Ti_{0.05})O_3$ anti-ferroelectric ceramics, Ceram. Int. **40** (2014) 5455-5460.

[9] B.A. Tuttle, D.A. Payne, The effects of microstructure on the electrocaloric properties of $Pb(Zr,Sn,Ti)O_3$ ceramics, Ferroelectrics **37** (1981) 603-606.

[10] J. Parui, S.B. Krupanidhi, Electrocaloric effect in antiferroelectric $PbZrO_3$ thin films, Phys.Stat.Sol. (RRL))-Rapid Research Letters **2** (2008) 230-232.

[11] X.H. Hao, Y. Wang, L. Zhang, L.W. Zhang, S.L. An, Composition-dependent dielectric and energy-storage-properties of (Pb,La)(Zr,Sn,Ti)O_3 antiferroelectric thick films, Appl. Phys. Lett. **102** (2013) 163903.

[12] X.H. Hao, J.W. Zhai, Electric-field tunable electrocaloric effects from phase transition between antiferroelectric and ferroelectric phase, Appl. Phys. Lett. **104** (2014) 022902.

[13] I.B. Misirlioglu, M. Alexe, L. Pintilie, D. Hesse, Space charge contribution to the apparent enhancement of polarization in ferroelectric bilayers and multilayers, Appl. Phys. Lett. **91** (2007) 022911.

[14] C. Wang, B.L. Cheng, S.Y. Wang, H.B. Lu, Y.L. Zhou, Z.H. Chen, G.Z. Yang, Improved dielectric properties and tunability of multilayered thin films of $(Ba_{0.80}Sr_{0.20})(Ti_{1-x}Zr_x)O_3$ with compositionally graded layer, Appl. Phys. Lett. **84** (2004) 765-767.

[15] L.W. Zhang, X.H. Hao, J.C. Yang, S.L. An, B. Song, Large enhancement of energy-storage properties of compositional graded $(Pb_{1-x}La_x)(Zr_{0.65}Ti_{0.35})O_3$ relaxor ferroelectric thick films, Appl. Phys. Lett. **103 (**2013) 113902.

[16] R.V.K. Mangalam, J.C. Agar, A.R. Damodaran, J. Karthik, L.W. Martin, Improved pyroelectric figures of merit in compositionally graded $PbZr_{1-x}Ti_xO_3$ thin films, ACS Appl. Mater. Interfaces **5** (2013) 13235-13241.

[17] X. J. Meng, J. L. Sun, J. Yu, H. J. Ye, S. L. Guo, and J. H. Chu, *Appl. Surf. Sci.*, **171**, 68 (2001).

[18] Q.P. Jia, B. Shen, X.H. Hao, J.W. Zhai, X. Yao, Enhanced dielectric property from highly (100)-oriented barium zirconate titanate compositional gradient films, Thin Solid Films **518** (2010) e89-e92.

[19] H.F. Ji, W. Ren, L.Y. Wang, P. Shi, X.F. Chen, X.Q. Wu, X. Yao, S.T. lau, Q.F. Zhou, K.K. Shung, Structure and electrical properties of $Na_{0.5}Bi_{0.5}TiO_3$ ferroelectric thick films derived

from a polymer modified sol-gel method, IEEE Trans. Ultrason. Ferroelectr. Freq. Control **58** (2011) 2042-2049.

[20] X.H. Hao, Y. Wang, J.C. Yang, S.L. An, J.B. Xu, High energy-storage performance in $Pb_{0.91}La_{0.09}(Zr_{0.65}Ti_{0.35})O_3$ relaxor ferroelectric thin films, J. Appl. Phys. **112** (2012) 114111.

[21] P. Khaenamkaew, I.D. Bdikin, A.L. Kholkin, S. Muensit, Microstructure and ferroelectric properties of sol-gel graded PZT (40/52/60) and (60/52/40) thin films, Ceram. Int. **34** (2008) 1027-1030.

[22] M. Ye, Q. Sun, X. Chen, Z. Jiang, F. Wang, Electrical and Energy storage performance of Eu-Doped $PbZrO_3$ thin films with different gradient sequences, J. Am. Ceram. Soc. **95** (2012) 1486-1488.

[23] D.Y. Wang, J. Wang, H.L.W. Chan, C.L. Choy, Structural and electro-optic properties of $Ba_{0.7}Sr_{0.3}TiO_3$ thin films grown on various substrates using pulsed laser deposition, J. Appl. Phys. **101** (2007) 043515.

[24] B. L. Peng, H. Q. Fan, and Q. Zhang, *Adv. Funct. Mater.*, 2013, **23**, 2987-2992.

[25] A. S. Mischenko, Q. Zhang, J. F. Scott, R. W. Whatmore, and N. D. Mathur, *Science*, 2006, **311**, 1270-1271.

[26] Y. Zhao, X. H. Hao, and Q. Zhang, *ACS Appl. Mater. Interfaces*, 2014, **6**, 11633-11639.

[27] R. Pirc, Z. Kutnjak, and R. Blinc, *Appl. Phys. Lett.*, 2011, **98**, 021909.

[28] E. Defay, S. Crossley, S. Kar-Narayan, X. Moya, N.D. Mathur, The electrocaloric efficiency of ceramic and polymer films, Adv. Mater. **25 (**2013) 3337-3342.

[29] X. Moya, E. Stern-Taulats, S. Crossley, D. González-Alonso, S. Kar-Narayan, A. Planes, L. Mañosa, N. D. Mathur, Giant electrocaloric strength in single-crystal $BaTiO_3$, Adv. Mater. **25** (2013) 1360-1365.

[30] B. Ma, D.K. Kwon, M. Narayanan, U.B. Balachandran, Leakage current characteristics and dielectric breakdown of antiferroelectric $Pb_{0.92}La_{0.08}Zr_{0.95}Ti_{0.05}O_3$ film capacitors grown on metal foils, J. Phys. D: Appl. Phys. **41** (2008) 205003.

[31] L. Zhang, X.H. Hao, Dielectric properties and energy-storage performances of $(1-x)(Na_{0.5}Bi_{0.5})TiO_3$-$xSrTiO_3$ thick films prepared by screen printing technique, J. Alloys Comp. **586** (2014) 674-678.

[32] S. Tong, B.H. Ma, M. Narayanan, S.S. Liu, R. Koritala, U. Balachandran, D.L. Shi, Lead lanthanum zirconate titanate ceramic thin films for energy storage, ACS Appl. Mater. Interfaces, **5** (2013) 1474-1480.

[33] C. Ang, Z. Yu, L.E. Cross, Oxygen-vacancy-related low-frequency dielectric relaxation and electrical conduction in Bi:$SrTiO_3$, Phys. Rev. B **62** (2000) 228-236.

Figure caption

Fig. 1 The schematic diagrams of (a) the single-composition, (b) up-graded, and (c) down-graded PLZT AFE thick films.

Fig. 2 XRD patterns of the up-graded, down-graded, and single-composition PLZT AFE thick films, respectively.

Fig. 3 Surface FE-SEM morphology images of (a) the up-graded (b), down-graded, and (c) single-composition PLZT AFE thick films. The inset is the corresponding cross-section images of these films.

Fig.4 Room temperature frequency-dependent dielectric constant and dielectric loss of the up-graded, down-graded, and single-composition PLZT AFE thick films.

Fig. 5 Dielectric constant as a function of dc voltage at 100 kHz of the up-graded, down-graded, and single-composition PLZT AFE thick films.

Fig. 6 Temperature dependence of dielectric constant of the up-graded, down-graded, and single-composition PLZT AFE thick films at 100 kHz.

Fig. 7 Room temperature *P*-*E* loops of the up-graded, down-graded, and single-composition PLZT AFE thick films at 1 kHz.

Fig. 8 (a) Electric-field dependence of recoverable energy-storage density and energy-storage efficiency of the up-graded, down-graded, and single-composition PLZT AFE thick films. (b) Temperature dependence of energy-storage density and energy-storage efficiency these films measured at 900 kV/cm.

Fig. 9 (a) The adiabatic temperature changes ΔT as a function of temperature under 900 kV/cm of the up-graded, down-graded, and single-composition PLZT AFE thick films. (b) The adiabatic

changes in entropy ΔS.

Fig. 10 (a) The temperature dependence of the electrocaloric coefficient of the up-graded, down-graded, and single-composition PLZT AFE thick films. (b) The temperature dependence of the refrigeration efficiency of these films.

Fig.11 (a) Dielectric relaxation current of the up-graded, down-graded, and single-composition PLZT AFE thick films under 400 kV/cm and room temperature. The inset is corresponding gradient sequence dependences of steady-state leakage current of the films. (b) Dielectric relaxation current of the up-graded film at different temperature. The inset gives the steady-state current density and corresponding fitting curve as a function of reciprocal temperature.

Fig. 1 Ye Zhao and Xihong Hao, *et.al.*

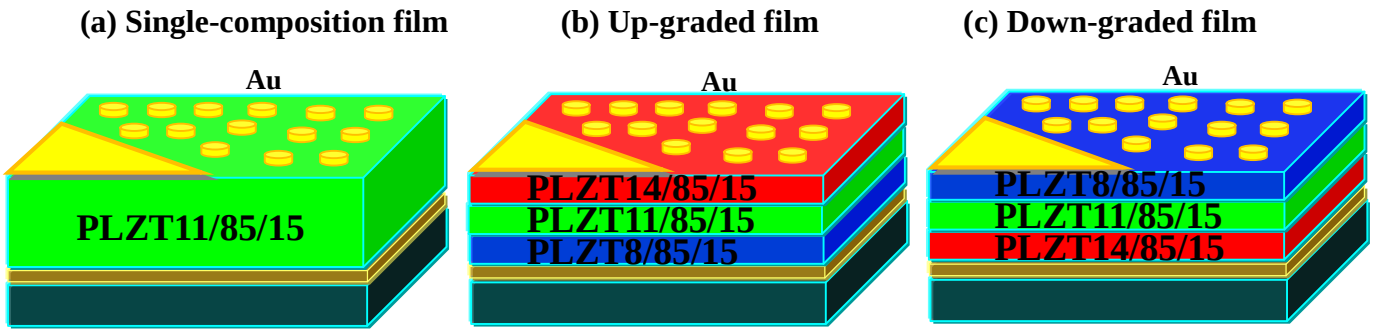

Fig. 2 Ye Zhao and Xihong Hao, *et.al.*

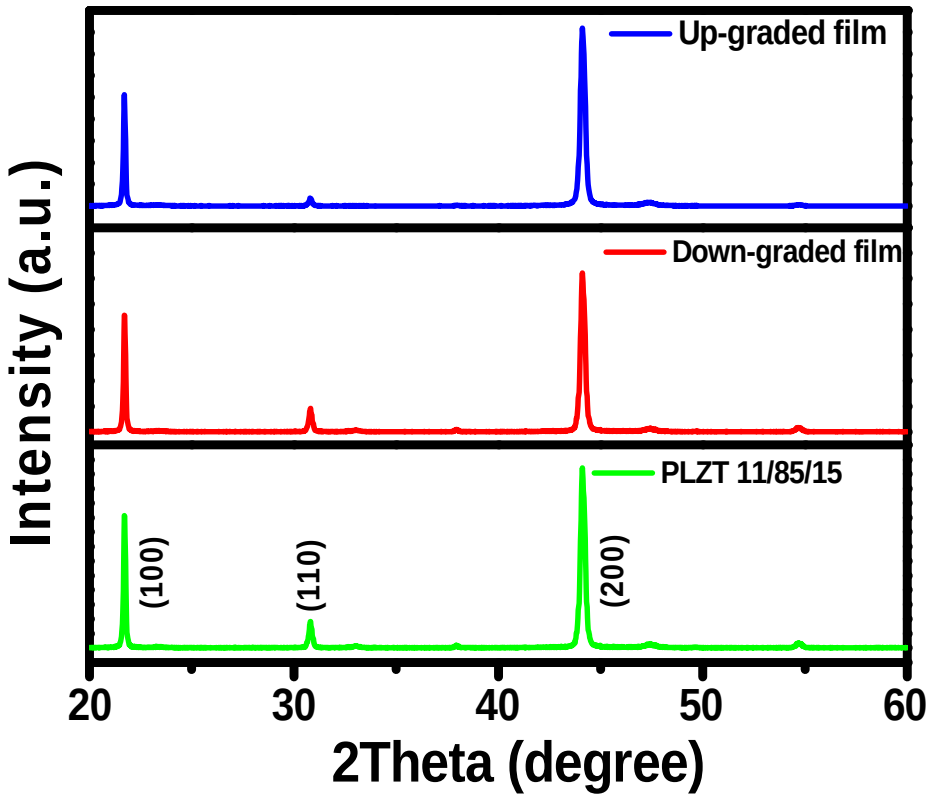

Fig. 3 Ye Zhao and Xihong Hao, *et.al.*

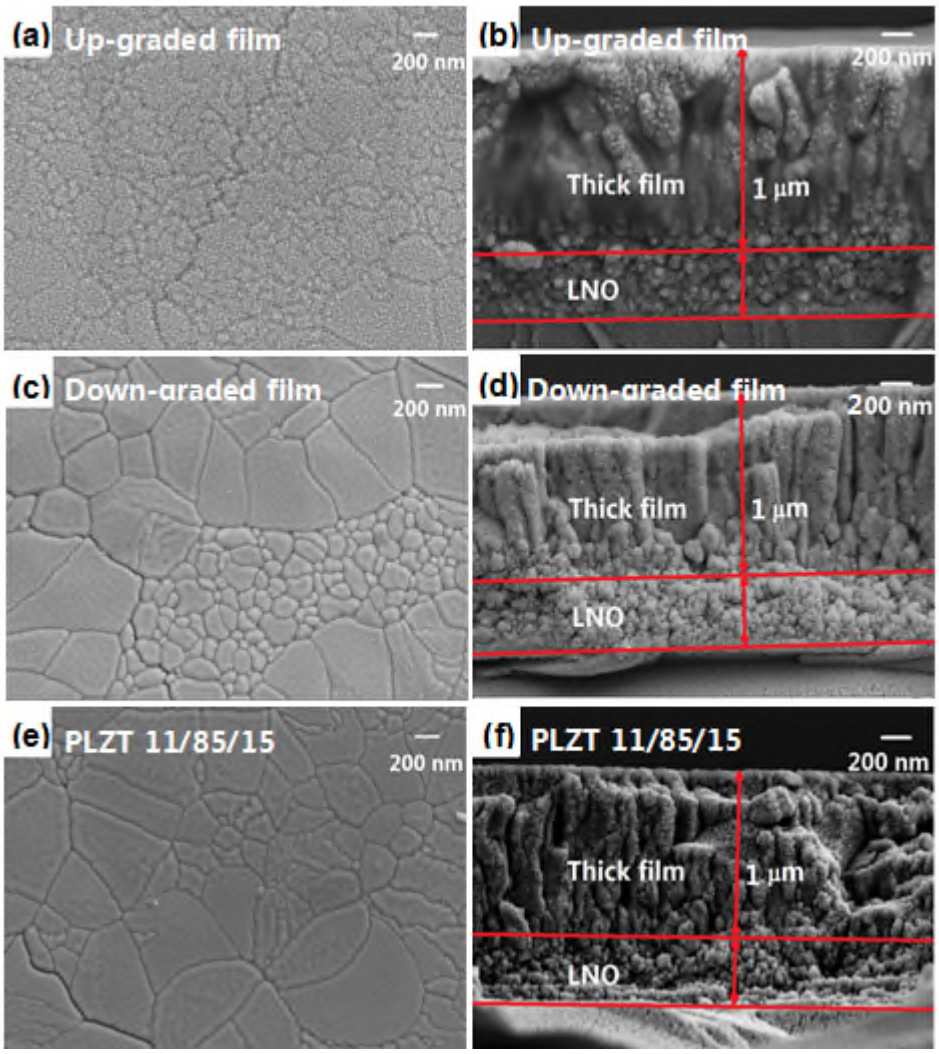

Fig. 4 Ye Zhao and Xihong Hao, *et.al.*

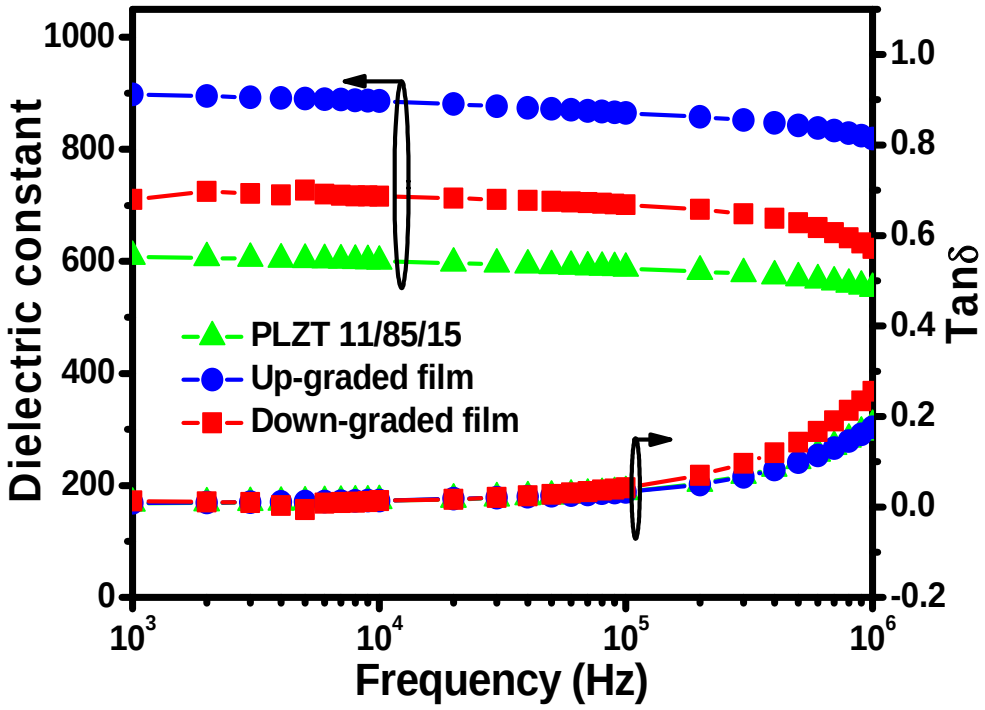

Fig. 5 Ye Zhao and Xihong Hao, *et.al.*

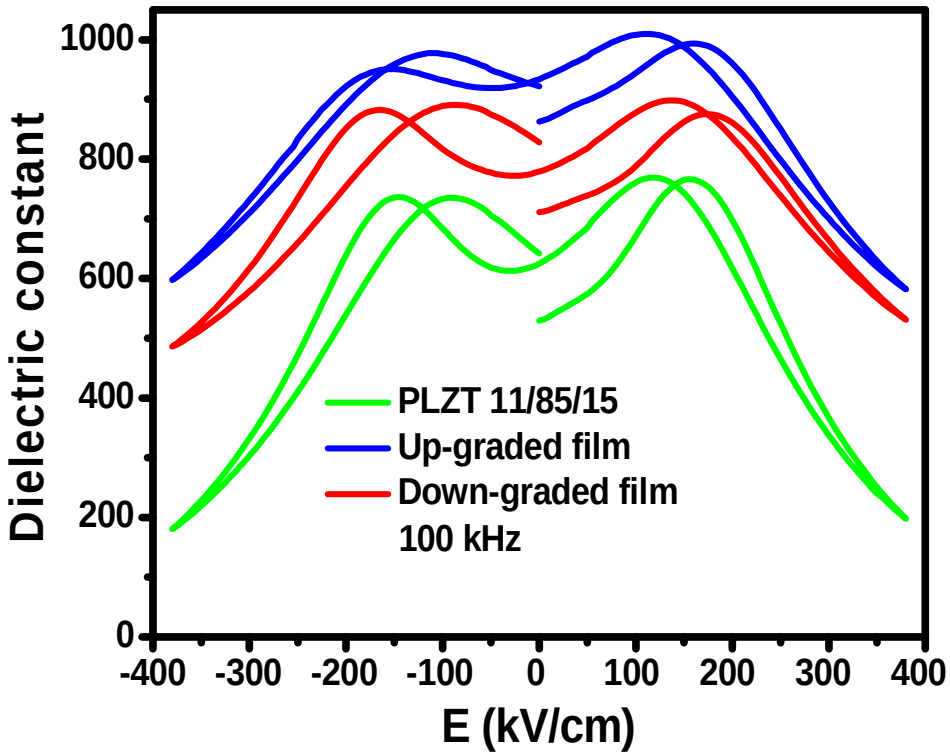

Fig. 6 Ye Zhao and Xihong Hao, *et.al.*

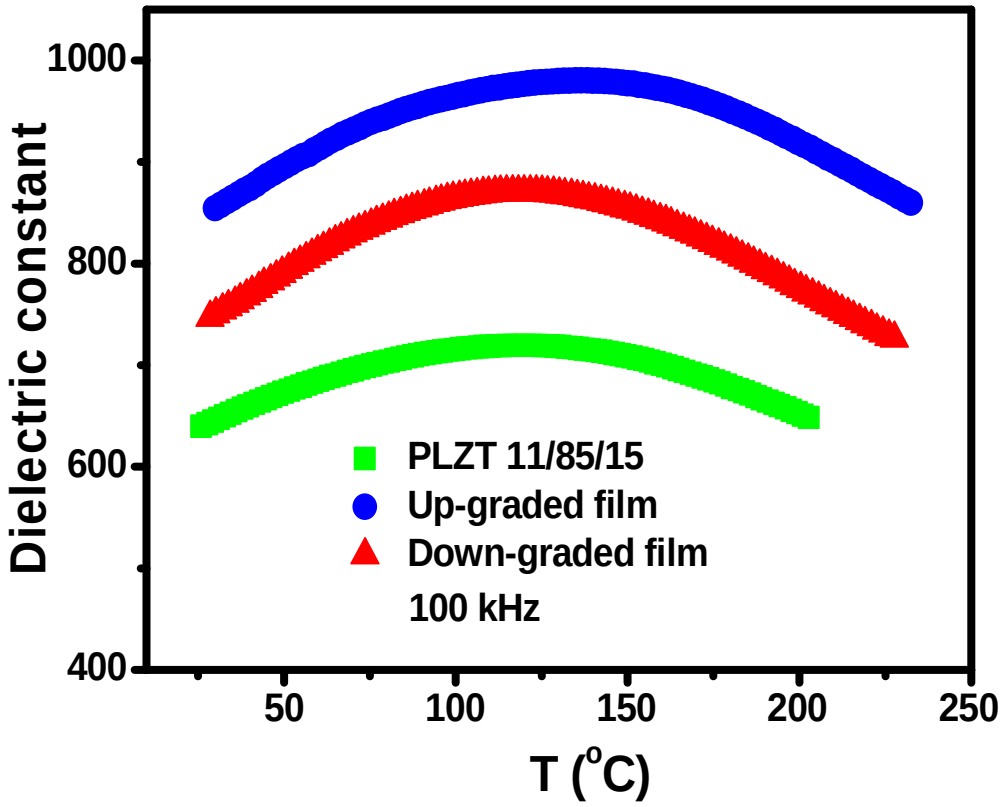

Fig. 7 Ye Zhao and Xihong Hao, *et.al.*

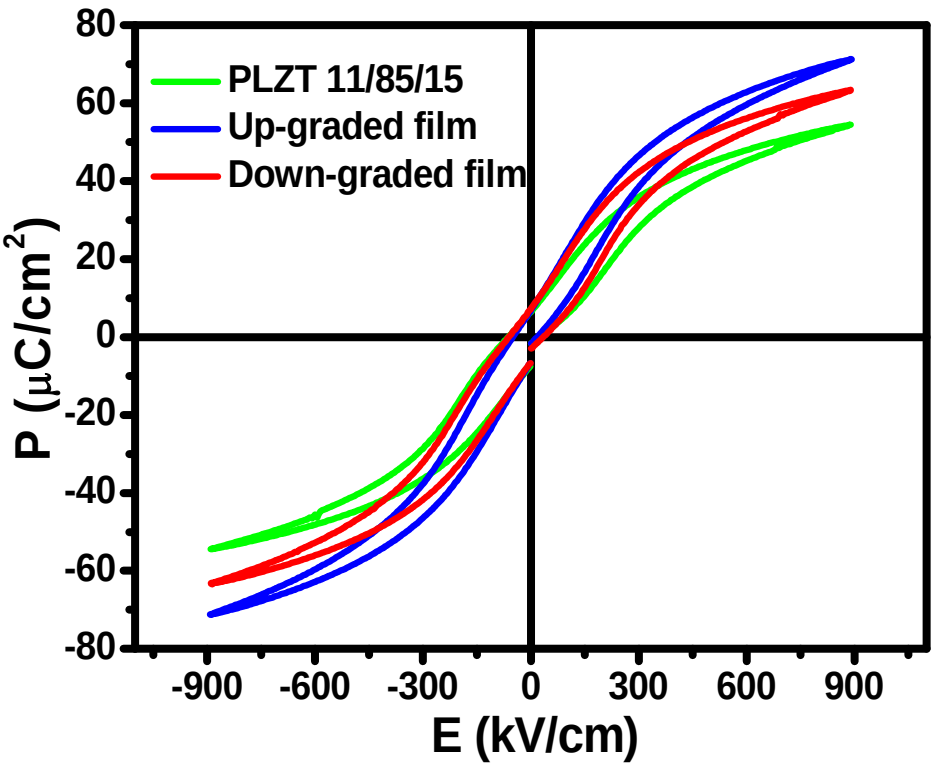

Fig. 8 Ye Zhao and Xihong Hao, *et.al.*

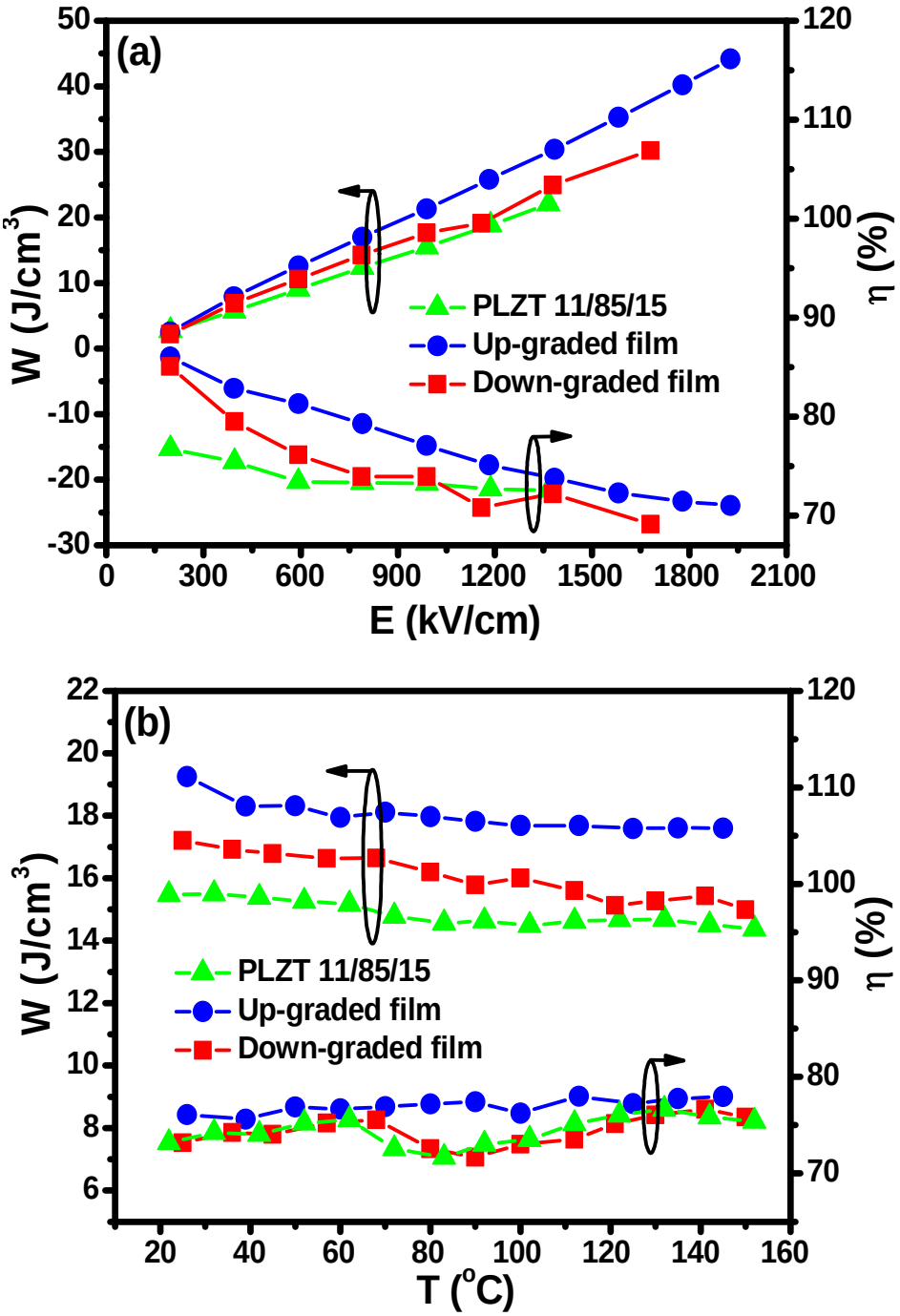

Fig. 9 Ye Zhao and Xihong Hao, *et.al.*

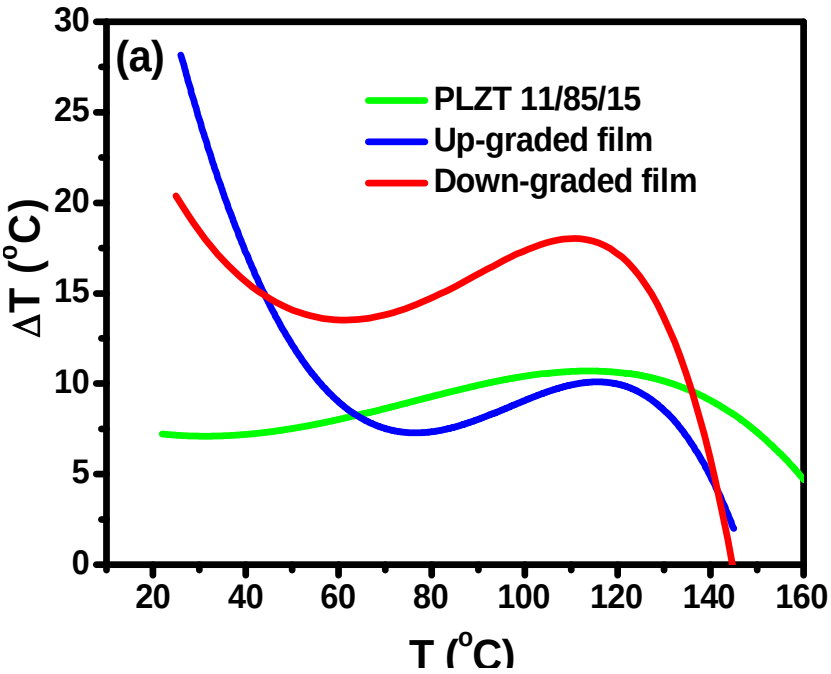

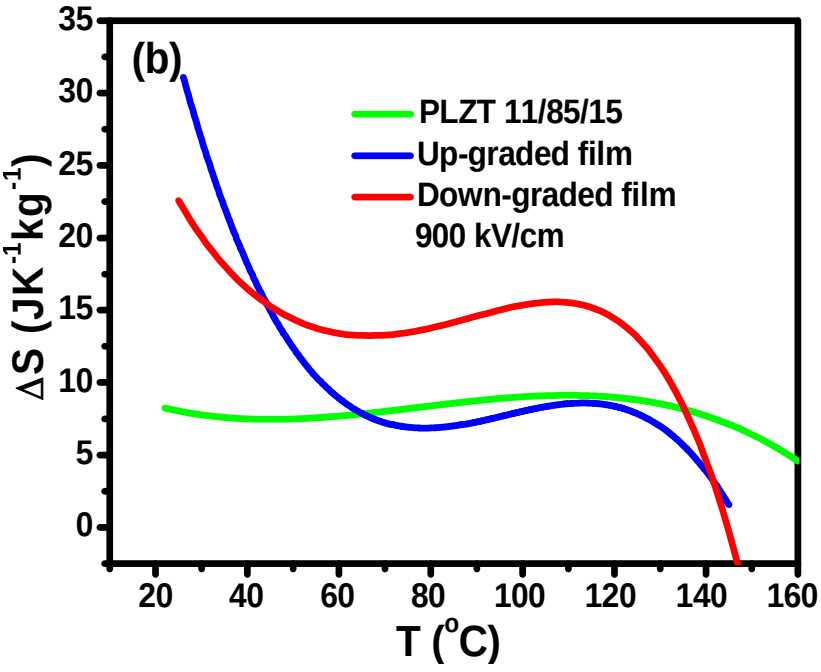

Fig. 10 Ye Zhao and Xihong Hao, *et.al.*

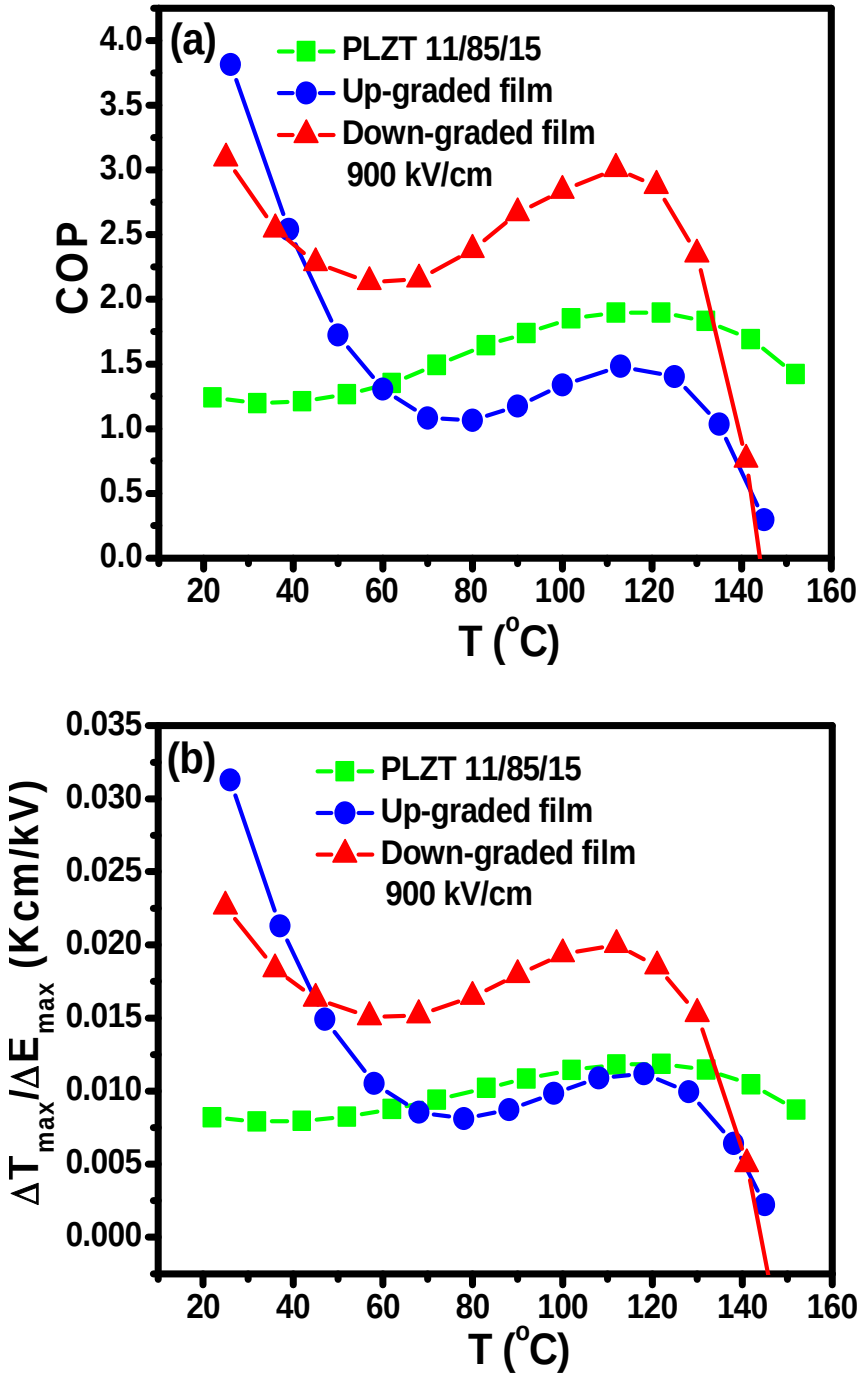

Fig. 11 Ye Zhao and Xihong Hao, *et.al.*

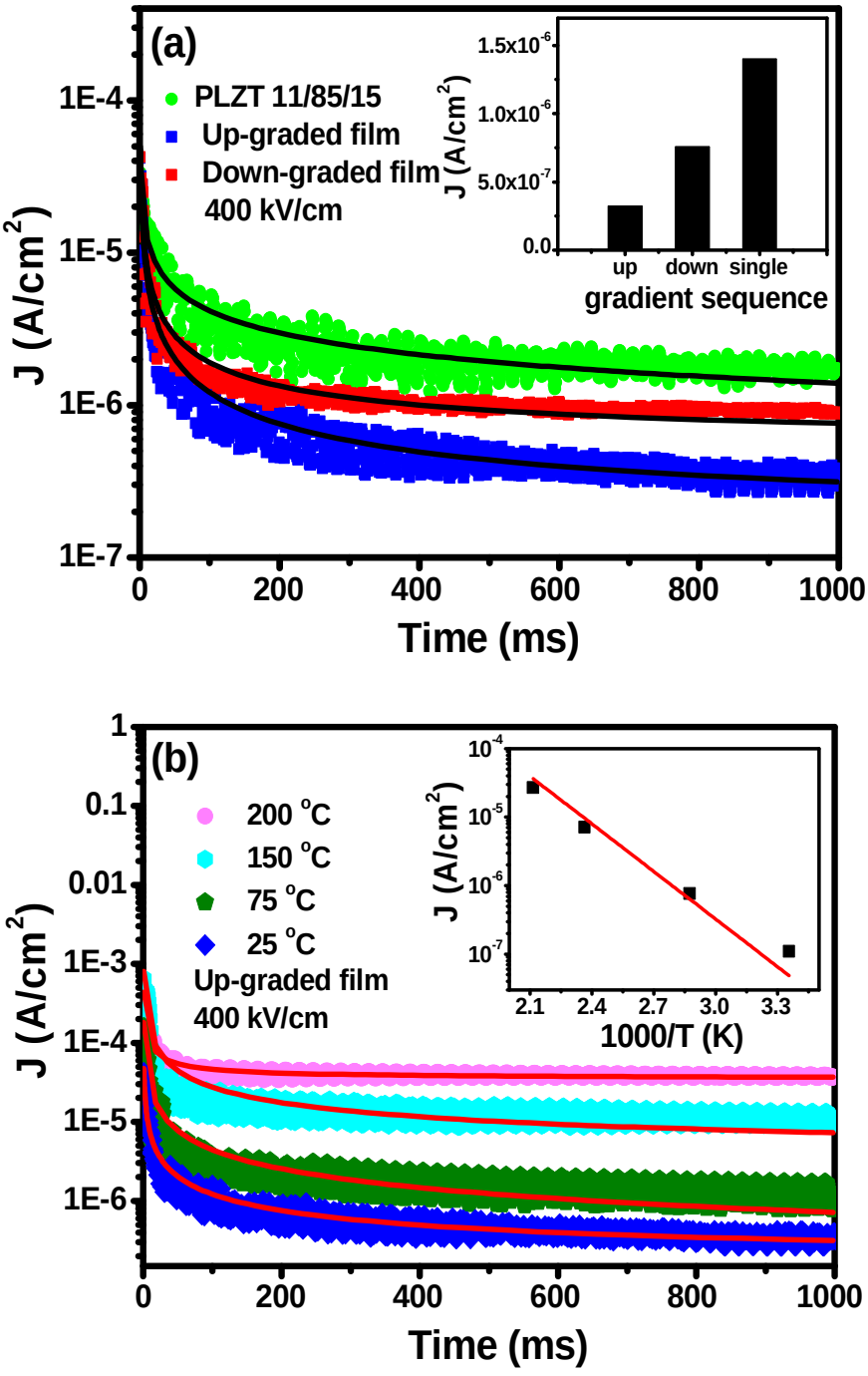

Table 1. The values of P_s, φ, Θ, C, and T for the up-graded, down-graded and single-composition PLZT AFE thick films.

	P_s ($\mu C/cm^2$)	Θ (10^7 K)	φ	C ($JK^{-1}\ kg^{-1}$)	T	P_s^2/Θ ($10^{-5}\mu C^2/Kcm^4$)
Up-graded film	73	2.5	6	330	RT	21.3
Down-graded film	63	2.6	6	330	RT	15.2
PLZT 11/85/15	54	4.6	6	330	RT	6.3